AIAA Meeting Papers on Disc, January 1997
A9715493, F49620-94-1-0019, F49620-95-1-0405, AIAA Paper 97-0432

Linear instability of compressible plane Couette flows

Sean Hu
California Univ., Los Angeles

Xiaolin Zhong
California Univ., Los Angeles

AIAA, Aerospace Sciences Meeting & Exhibit, 35th, Reno, NV, Jan. 6-9, 1997

The stability of compressible plane Couette flow, which is a simple case of hypersonic wall-bounded shear flows, is not well understood even though incompressible Couette flow has been studied extensively by linear stability analysis and shown to be stable to linear disturbances. As a first step in studying the stability of 3D hypersonic boundary layers, we study the temporal stability of compressible Couette flows with a perfect gas model. The full compressible linear stability equations are solved by both a high-order finite-difference global method and a Chebyshev spectral collocation global method. The accuracy of the linear stability codes are validated by comparing the solutions from the two approaches with known solutions for compressible boundary layer. Unstable first and second modes are found for compressible Couette flow at finite Reynolds numbers. The inviscid second modes are found to be the dominant instability. The results are consistent with the prediction that unstable modes are possible for compressible Couette flow. The second modes are found to be 2D, and stabilized by viscosity. (Author)

Linear Instability of Compressible Plane Couette Flows

Sean Hu *and Xiaolin Zhong †
University of California, Los Angeles, California 90095

Abstract

The stability of compressible plane Couette flow, which is a simple case of hypersonic wall-bounded shear flows, is not well understood even though incompressible Couette flow has been studied extensively by linear stability analysis and shown to be stable to linear disturbances. As a first step in studying the stability of three-dimensional hypersonic boundary layers, this paper studies the temporal stability of compressible Couette flows with a perfect gas model. The full compressible linear stability equations are solved by both a high-order finite-difference global method and a Chebyshev spectral collocation global method. The accuracy of the linear stability codes are validated by comparing the solutions from the two approaches with known solutions for compressible boundary layer. Unstable first and second modes are found for compressible Couette flow at finite Reynolds numbers. The inviscid second modes are found to be the dominant instability. The results are consistent with the prediction by Duck et al. that unstable modes are possible for compressible Couette flow. The second modes are found to be two-dimensional and are stabilized by viscousity. The Mach number corresponding to the most unstable second modes increase with Reynolds number but has a finite limit. The second modes are destabilized first by wall cooling and then stabilized by further reduction of the lower wall temperature. This is different with what is known for boundary layer second mode instability. The first mode instability characteristics are also discussed in this paper.

1 Introduction

The understanding of the stability and transition mechanism of high-speed flows are critical to the accurate calculations of aerodynamic forces and heatings to supersonic and hypersonic vehicles. Current understanding of the laminar-turbulent transition in compressible boundary layers comes mainly from the parallel linear stability theory[1, 2, 3, 4]. Mack[2] did extensive work on the linear stability of two and three-dimensional supersonic boundary layers and shear flows. One of the most important contributions by Mack to the compressible linear theory is that he discovered a new family of higher modes at supersonic speeds. He showed that, for compressible boundary layer stability, the lowest-frequency two-dimensional second mode (Mack mode) is the most unstable one for Mach number greater than about 4.

The linear stability theory provides many insights to the stability properties of compressible boundary layers. It also serves as a convenient meanings in analyzing the stability characteristic of various flows. However, it neglects non-parallel effects of the boundary layer and confines the problem to the initial growth of the disturbances at a local station of the boundary layer. In reality, the thickness of the boundary layers grows downstream, and the transition process continues as the amplitude of the disturbances increases. Nonlinear interactions between disturbances occur to cause the rapid growth of the disturbance and eventually the breakdown to turbulence. Furthermore, for three-dimensional boundary layers, it has been shown experimentally[5, 6, 7] that cross-flow instability, nonlinear interaction of modes, and distortions of the basic flow are important in the transition process. Although the experiments were conducted in the low Mach number regime, it is reasonable to speculate that similar phenomena may occur in the supersonic and hypersonic flow regime. The linear stability theory and the e^N method[8, 9] for transition prediction can not account for these physical phenomena properly. The remedies in these situations are the direct numerical simulation (DNS) method [10] and the Parabolized Stability Equations (PSE) method developed by Bertolotti and Herbert[11, 12, 13]. The DNS method is accurate but computationally more expensive comparing to the PSE method. In the PSE method, spatial evolution of disturbances are computed by an efficient space marching algorithm. The PSE method has been successfully applied to many subsonic and supersonic boundary layers.

To understand the supersonic and hypersonic flow

*Graduate Student,
†Assistant Professor, Mechanical and Aerospace Engineering Department, Member AIAA

transition, accurate linear stability analysis codes are needed in conjunction with DNS or PSE tools to provide initial conditions as well as physical insights. In developing these codes, temporal linear stability of compressible Couette flow is chosen as the objective since it is not yet well understood. Not many results, numerical or experimental, with regard to the stability of compressible Couette flow exist. Therefore, more elaboration is required on the validation of results. We have hence developed two global stability computer codes. One uses a Chebyshev spectral collocation method[14], the other uses a fourth-order finite-difference method. The accuracy of the linear stability codes are validated by comparing the solutions of compressible flat plate boundary layer with known solutions in Malik[14]. The accuracy of the calculations on compressible Couette flow are ensured by comparing the solutions from both methods.

Extensive work has been done with regard to incompressible plane Couette flow previously due to the existence of a simple exact solution of the Navier-Stokes equations. The first general proof of stability was given by Romanov[15]. However, instabilities were observed in experiments. [16, 17]. A number of investigations have been made to resolve the dichotomy. The evidence seems to point to the finite-amplitude (nonlinear) effects. The compressible stability of plane Couette flow, on the other hand, is much less well understood. Glatzel[18, 19] studied this problem under the assumptions of constant viscosity, density and pressure, which led to constant temperature. Girard[20] considered the same problem allowing for variations in density and pressure. Duck et al.[21] solved the two-dimensional small-amplitude disturbance equations numerically for the same problem at finite Reynolds numbers using a proper perfect gas model, and investigated its stability at the inviscid limit. They found unstable second modes in the inviscid limit but they didn't obtain unstable modes in the viscous computations. We compared the results of our numerical codes with some of those in [21] and conducted viscous computations over a range of Mach numbers and wave numbers at finite Reynolds numbers. As a result, unstable modes were discovered at finite Reynolds numbers for a range of Mach numbers and wave numbers. The unstable modes found are the inviscid first modes and second modes. Since unstable second modes are dominant for compressible Couette flow, their characteristics were investigated thoroughly on the effects of compressibility, three-dimensionality, and wall cooling. The results of the linear stability analysis are used to check with the direct numerical simulation results by Zhong[22] and will eventually serve as initial conditions for PSE simulations of the transition for compressible flows.

2 Compressible Linear Stability Formulation

Three-dimensional Navier-Stokes equations for a perfect gas model upon which current stability results are based can be found in Malik[14]. It's given below for completeness.

$$\rho[\frac{\partial q}{\partial t} + (q \cdot \nabla)q] = -\nabla p + \nabla \cdot [\lambda(\nabla \cdot q)\bar{\bar{I}} + \nabla \cdot [\mu(\nabla q + \nabla q^{tr})], \quad (1)$$

$$\frac{\partial \rho}{\partial t} + \nabla \cdot (\rho q) = 0, \quad (2)$$

$$\rho c_p[\frac{\partial \tau}{\partial t} + (q \cdot \nabla)\tau] = \nabla \cdot (k \nabla \tau) + \frac{\partial p}{\partial t} + (q \cdot \nabla)q + \Phi, \quad (3)$$

$$p = \rho \mathcal{R} \tau, \quad (4)$$

where q is the velocity vector, ρ the density, p the pressure, τ the temperature, $\mathcal{R}$ the gas constant, c_p the specific heat, k the thermal conductivity, μ the first coefficient of viscosity, and λ the second coefficient of viscosity. The viscous dissipation Φ is given as

$$\Phi = \lambda(\nabla \cdot q)^2 + \frac{\mu}{2}[(\nabla q + \nabla q^{tr})]^2. \quad (5)$$

For Couette flow, a compressible Newtonian perfect fluid is confined between two infinite parallel planes defined by $y = 0$ (lower wall) and $y = L$ (upper wall). The upper wall has velocity U_∞ (the unperturbed upper wall properties are denoted by a subscript ∞), taken parallel to the plane of the wall, while the lower wall is stationary. We non-dimensionalize velocities by U_∞, lengthscales by L, density by ρ_∞, temperature by τ_∞, and pressure by $\rho_\infty U_\infty^2$. The dimensional timescale is L/U_∞. The Reynolds number is defined by

$$Re = \frac{U_\infty \rho_\infty L}{\mu_\infty}, \quad (6)$$

the Mach number M_∞ by

$$M_\infty = \frac{U_\infty}{(\gamma R \tau_\infty)^{\frac{1}{2}}}, \quad (7)$$

where $R = c_p - c_v$, and c_p and c_v are the specific heats at constant pressure and volume respectively, γ is the

ratio of specific heats taken to be 1.4. The Prandtl numer is defined by $Pr = \mu c_p/k$ and assumed to be a constant 0.72. We assume that viscosity depends solely on temperature, and Sutherland's law holds,

$$\mu = T^{1.5}(\frac{1+C}{T+C}), \tag{8}$$

where C is a constant taken to be 0.5 in this paper. Finally, $\lambda = -2/3\mu$ is assumed throughout the paper. Note that some linear stability computation is also done for the boundary layer case in comparison with Malik's results[14], where Reynolds number, the constant C in Sutherland's law, and some other details differ from those mentioned above. However, the linear stability equations derived below is universal with the exception of main flow parameters and boundary conditions.

The stability analysis is based on a normal mode analysis of perturbation equations of the nondimensionalized nonlinear governing equations. The perturbation equations are derived by representing the instantaneous flow variables as a sum of a mean and a fluctuation quantity, i.e.

$$\begin{gathered} u = \bar{U} + u',\ v = \bar{V} + v',\ w = \bar{W} + w' \\ p = \bar{p} + p',\ \tau = \bar{T} + T'. \end{gathered} \tag{9}$$

Substituting equation (9) into the nondimensional form of the governing equations (1) to (5) yields the perturbation equations (for details see Malik [14]). One may then apply the "locally parallel flow assumption" to the linearized perturbation equations assuming that the fluctuations of flow quantities are represented by harmonic waves of the following form:

$$\begin{gathered} (u', v', p', T', w') = [\hat{u}(y), \hat{v}(y), \hat{p}(y), \\ \hat{T}(y), \hat{w}(y)] exp[i(\alpha x + \beta z - \omega t)], \end{gathered} \tag{10}$$

where α, β are wavenumbers and ω is the frequency of the disturbance waves. These parameters are in general complex numbers. The notation for the complex amplitude function of a typical flow variable, say u, is $\hat{u}(y)$. Since we focused on the temporal linear stability of the compressible flows in current research, α, β are given as real constants while ω is an unknown complex parameter and to be solved for. The real part of ω, $\mathrm{Re}\{\omega\}$, represents the frequency of the disturbance while the imaginary part, $\mathrm{Im}\{\omega\}$, represents the amplification rate. When $\mathrm{Im}\{\omega\}$ is greater then 0, the disturbance is unstable. Substituting equation (10) into the linearized perturbation equations, leads to the following system of ordinary differential equations:

$$(AD^2 + BD + C)\Phi = 0, \tag{11}$$

where

$$\Phi = \{\hat{u}(y), \hat{v}(y), \hat{p}(y), \hat{T}(y), \hat{w}(y)\}^T. \tag{12}$$

and A, B and C are 5 x 5 matrices given in [14]. The operator D is the derivative operator d/dy in the wall-normal direction. The temporal stability analysis solves ω and $[\hat{u}(y), \hat{v}(y), \hat{p}(y), \hat{T}(y), \hat{w}(y)]^T$ as eigenvalues and eigenfunctions of the homogeneous boundary value problem given by equation (11). The eigenvalue problem was solved by a fourth-order finite-difference method and a spectral collocation method described in the following section.

3 Numerical Methods for Stability Equations

Various numerical methods for solving the linear stability equations of the hypersonic boundary layers were discussed and compared by Malik[14]. We used a fourth-order global finite-difference method (4FD) to compare with the second-order finite-difference scheme (2FD) and the Chebyshev spectral collocation method (SC) described in Malik[14].

3.1 Fourth-Order Finite-Difference Global Method

In the finite-difference method, equation (11) is discretized by finite difference approximation to the derivatives. Malik[14] used a staggered mesh for the second-order finite-difference scheme to avoid using the boundary values of $\hat{p}$ which are unknown. In implementing the fourth-order finite-difference method, we use a non-staggered grid. One-sided difference formulas which do not involve the wall points are used to approximate the first derivative of $\hat{p}$. The fourth-order finite-difference formulas at a grid point j, where j is from 1 to $N+1$, are the following.
For j from 3 to $N-1$,

$$\begin{gathered} D^2\Phi_j = \frac{1}{12\Delta y^2} \\ (-\Phi_{j+2} + 16\Phi_{j+1} - 30\Phi_j + 16\Phi_{j-1} - \Phi_{j-2}), \end{gathered} \tag{13}$$

$$D\Phi_j = \frac{1}{12(\Delta y)} (-\Phi_{j+2} + 8\Phi_{j+1} - 8\Phi_{j-1} + \Phi_{j-2}). \quad (14)$$

For $j = 2$:

$$D^2\Phi_j = \frac{1}{12(\Delta y)^2}(10\Phi_{j-1} - 15\Phi_j - 4\Phi_{j+1} + 14\Phi_{j+2} - 6\Phi_{j+3} + \Phi_{j+4}), \quad (15)$$

$$D\Phi_j = \frac{1}{12(\Delta y)}(-3\Phi_{j-1} - 10\Phi_j + 18\Phi_{j+1} - 6\Phi_{j+2} + \Phi_{j+3}). \quad (16)$$

For $j = N$:

$$D^2\Phi_j = \frac{1}{12(\Delta y)^2}(\Phi_{j-4} - 6\Phi_{j-3} + 14\Phi_{j-2} - 4\Phi_{j-1} - 15\Phi_j + 10\Phi_{j+1}), \quad (17)$$

$$D\Phi_j = \frac{1}{12(\Delta y)}(-\Phi_{j-3} + 6\Phi_{j-1} - 18\Phi_{j-1} + 10\Phi_j + 3\Phi_{j+1}). \quad (18)$$

The first derivative of $\hat{p}$ near the wall are given below. For $j = 2$:

$$D\Phi_j = \frac{1}{12(\Delta y)}(-25\Phi_j + 48\Phi_{j+1} - 36\Phi_{j+2} + 16\Phi_{j+3} - 3\Phi_{j+4}). \quad (19)$$

For $j = 3$:

$$D\Phi_j = \frac{1}{12(\Delta y)}(-3\Phi_{j-1} - 10\Phi_j + 18\Phi_{j+1} - 6\Phi_{j+2} + \Phi_{j+3}). \quad (20)$$

For $j = N$:

$$D\Phi_j = \frac{1}{12(\Delta y)}(3\Phi_{j-4} - 16\Phi_{j-3} + 36\Phi_{j-2} - 48\Phi_{j-1} + 25\Phi_j). \quad (21)$$

For $j = N - 1$:

$$D\Phi_j = \frac{1}{12(\Delta y)}(-\Phi_{j-3} + 6\Phi_{j-2} - 18\Phi_{j-1} + 10\Phi_j + 3\Phi_{j+1}). \quad (22)$$

When equation (11) is discretized using the 4FD formulas given above, along with the boundary conditions for compressible Couette flow:

$$\begin{aligned} &\hat{u}(0) = \hat{v}(0) = \hat{w}(0) = 0, \\ &\hat{u}(1) = \hat{v}(1) = \hat{w}(1) = 0, \\ &\frac{\partial \hat{T}}{\partial y}(y = 0) = 0, \hat{T}(1) = 0, \end{aligned} \quad (23)$$

a matrix eigenvalue problem is formed:

$$A'\Phi = \omega B'\Phi, \quad (24)$$

where ω is the eigenvalue and Φ is the discrete represention of the eigenfunction. The eigenvalue problem is then solved using the QZ eigenvalue algorithm in the IMSL computer library.

A natural choice for the stretching function in solving Couette flow is

$$y = \frac{1 - cos\pi\eta}{2}, \quad (25)$$

where $\eta \in [0, 1], y \in [0, 1]$. However, this transformation has a singularity in $\partial\eta/\partial y$. A modified transformation is thus used given below:

$$y = \frac{cos\pi\eta - cos\pi\Delta}{cos[\pi(1 - \Delta)] - cos\pi\Delta}, \quad (26)$$

where Δ is chosen to be 0.001 and $\eta \in [\Delta, 1 - \Delta], y \in [0, 1]$.

3.2 Chebyshev Spectral Collocation Global Method

The discretization formulas for equation (11) using the Chebychev spectral collocation method can be found in Malik[14] and are given below for completeness. The Nth-order Chebyshev polynomials T_N are defined on the interval $j \in [-1, 1]$. The collocation points ξ_j, which are the extrema of T_N, are

$$\xi_j = cos\frac{\pi j}{N}, \quad j = 0, 1, \ldots, N. \quad (27)$$

In order to apply the spectral collocation method, an interpolant polynomial is constructed for the dependent variables in terms of their values at the collocation points. An Nth-order polynomial is

$$\phi(\xi) = \sum_{k=0}^{N} \lambda_k(\xi)\phi(\xi_k), \quad (28)$$

where the interpolant $\lambda_k(\xi)$ for the Chebyshev scheme is

$$\lambda_k(\xi) = (\frac{1 - \xi^2}{\xi - \xi_k})\frac{T_N(\xi)}{N^2 c_k}(-1)^{(k+1)}, \quad (29)$$

where $c_0 = c_N = 2$, and $c_k = 1$, $0 < k < N$.

The first derivative of $\phi(\xi)$ may be written as

$$\left.\frac{d\phi}{d\xi}\right|_j = \sum_{k=0}^{N} E_{jk}\phi_k, \tag{30}$$

where E_{jk} are the elements of the derivative matrix defined as:

$$E_{jk} = \frac{c_j}{c_k}\frac{(-1)^{k+j}}{\xi_j + \xi_k}; \qquad j \neq k, \tag{31}$$

$$E_{jj} = \frac{\xi_j}{2(1-\xi_j^2)}, \tag{32}$$

$$E_{00} = -E_{NN} = \frac{2N^2+1}{6}, \tag{33}$$

The transformation between physical and computational domains is

$$\xi_j = 2y_j - 1, \qquad \text{where} \quad y \in [0,1], \tag{34}$$

which clusters the grid points close to both walls. The scaling factor for the transformation between physical domain y and computational domain ξ is given as

$$S_j = \left.\frac{\partial\xi}{\partial y}\right|_j = 2; \qquad j = 0,1,...,N, \tag{35}$$

then the first derivative matrix F in the physical domain may be written as

$$F_{jk} = S_j E_{jk}, \tag{36}$$

and the second derivative matrix G_{jk} is

$$G_{jk} = F_{jm}F_{mk}. \tag{37}$$

Now the governing equation (11) may be written at the collocation points as

$$A_j\sum_{k=0}^{N} G_{jk}\phi_k + B_j\sum_{k=0}^{N} F_{jk}\phi_k + C_j\phi_j = 0. \tag{38}$$

The Neumann boundary condition for temperature at the lower wall is enforced using:

$$\left.\frac{dT}{dy}\right|_{y=0} = \sum_{k=0}^{N} F_{Nk}T_k = 0. \tag{39}$$

The Neuman conditions on pressure are enforced as

$$\left.\frac{\partial p}{\partial y}\right|_{y=0} = a, \quad \left.\frac{\partial p}{\partial y}\right|_{y=1} = b, \tag{40}$$

where a and b are evaluated at the two boundaries using the normal momentum equations. Now the same matrix eigenvalue problem is formed as in equation (24) except that Φ contains $5N-2$ elements instead of $5N-4$ elements as in the 4FD scheme. Again, the eigenvalue problem is solved by an IMSL subroutine.

4 Comparisons of Code Performance

We first checked our linear stability codes by comparing the linear stability solutions from both approaches for flat-plate boundary layer to the known solutions in Malik[14]. The only differences in solving the linear stability of compressible boundary layer and Couette flow are the main flow and possibly the boundary conditions. Indeed, once the accurate main flow profiles are obtained and the proper boundary conditions used, the linear stability codes can be used to solve for the linear stability problem of any flow. In our case, besides the main flow profiles, the only difference in solving the linear stability of boundary layer and Couette flow is the treatment of temperature perturbation at the lower boundary. Malik[14] used $\hat{T} = 0$ for boundary layer. We used Neuman condition for temperature perturbation at the lower wall to be consistent with Duck et al.[21].

Malik[14] uses various numerical schemes to solve for the boundary layer linear stability problem. For each schemes, both global and local methods are used in solving the problem. A global method computes all the eigenvalues of the discretized system, while a local method purifys the eigenvalues obtained by the global methods and the associated eigenfunctions. Good accuracy may be achieved using less grid points when both methods are used. Since our numerical codes are global methods, more grid points are used in comparing our results with those from Malik[14]. Malik[14] has 5 test cases for temporal linear stability of boundary

	Re	Im
4CD($N = 61$)	0.0367321	0.0005847
SDSP($N = 61$)	0.0367339	0.0005840
MDSP($N = 61$)	0.0367340	0.0005840
SC($N = 100$)	0.0367337	0.0005845
4FD($N = 100$)	0.0367338	0.0005840

Table 1: Real and imaginary parts of the eigenvalue ω for test case 3, $\alpha = 0.06, \beta = 0.1$

layer. Comparisons for all cases are similar. The comparisons for test case 3 are shown in Table 1 as an example. The conditions for test case 3 are Mach number 2.5, $Re = 3000, T_0 = 600^0 R$. In Table 1, 4CD, SDSP and MDSP are the methods used in Malik [14]. 4FD is our fourth-order finite-difference global method, SC the spectral collocation global method. Note SC is the same as the global SDSP in Malik [14]. 4FD uses an exponential stretching function for boundary layer. The stretching function for SC follows the stretching function described in Malik[14] for SDSP. From Table 1, one sees that our numerical results agree very well with Malik's results. 4FD method seems to perform better than SC method does in this case. However, this is not a general conclusion because the performance depends on the stretching function, the shape of the main flow profiles and hence flow conditions.

To validate the linear stability solutions for compressible Couette flow, we compared the eigenvalue spectra and eigenfunctions of the temporal linear stability equations resolved by both methods at various flow conditions. In the comparisons, phase velocity c, which is ω/α, is more often used instead of ω to be consistent with [21]. Furthermore, unless specified otherwise, β is set to zero in all cases. Figure 1 compares the phase velocity spectra at $M_\infty = 2.0, Re = 2 \times 10^5$, and $\alpha = 0.1$ computed using the the 2FD method, the 4FD method, and the SC method along with the result by Duck et al[21] as shown in Fig. 1 c). All our calculations use 100 grid points. The streamwise-velocity eigenfunctions of the least stable mode computed by both the 4FD method and the SC method are shown in Fig. 2. The comparisons show clearly that the results from the 4FD method and the SC method agree very well with each other. On the other hand, the 2FD method does not resolve the spectrum as accurately as the 4FD and the spectral methods do. Graphical comparisons of the eigenvalue spectra can also be made between our results and those in [21], even though they did not solve the z-momentum equation and therefore didn't include the z-direction modes in their results. As an example, the eigenvalue spectrum in Fig. 2 d) of [21] shown in Fig 1 c) agrees well with those in Fig. 1 b) with the exception of z-direction modes.

Spurious modes were reported in Malik[14] for global SDSP method. Since both our methods are global methods, spurious modes are also observed in the results from both 4FD and SC methods. Fortunately spurious modes are easy to identify because different methods usually give different spurious modes. Lastly, it is worth noting that when the eigenvalue and eigenfunctions for compressible Couette flow resolved by our linear stability codes are used to check with the DNS simulation conducted by Zhong[22], excellent agreement is obtained (details see Zhong[22]). Once the accuracy of the numerical codes were validated, the stability characteristics of compressible Couette flow was studied.

5 Stability of Compressible Couette Flow

The stability of compressible Couette flow was studied by Duck et al [21] solving proper equations. They did extensive analysis in the inviscid regime of the problem. Our focus is thus the viscous linear stability solution of the problem. Since the linear stability results on the boundary layer are more well-known, we also compare the Couette flow stability characteristics with those of boundary layer.

The effects of Mach number and Reynolds number in resolving the eigenvalue spectra

The effects of Mach number and Reynolds number on the phase velocity spectra are illustrated in Fig. 3, where the phase velocity spectra corresponding to $Re = 5 \times 10^5$ and 5×10^6 are shown for Mach 5 and Mach 10 respectively. The results show that as Reynolds number increases, the numerical resolution for the eigenvalues in the neighborhood of the triple point of the "Y" structure, which are of viscous nature, become less adequate. This phenomenon agrees with the conclusion by Reddy et al.[23] that this region of spectra is sensitive to very small errors in the linear matrix elements. As a consequence, more accurate schemes and more grid points are required in the computations in order to resolve the eigenvalues in that region. On the other hand, the numerical accuracy of the least stable modes, which are above the triple point region and of inviscid nature, is very good. Based upon the comparisons of the eigenvalue modes in the neighborhood of the triple points computed by both methods, one sees that the SC method outperformed

the 4FD method for the same number of grid points. Furthermore, at high Reynolds numbers, the difference between the spectra resolved using both methods becomes large. The effects of Mach number on the spectra can be seen by comparing Fig. 3 b) and 3 d) as an example. It is observed that as M_∞ increases, the eigenvalues in the neighborhood of the triple point become easier to resolve for a fixed Reynolds number.

Neutral Stability Contours

After the validation of the accuracy of the 4FD and SC methods, viscous computations were conducted over a range of Mach numbers and wave numbers including the region where instability has been found in the inviscid limit by Duck et al.[21]. As a result, unstable modes have been found at finite Reynolds numbers using both the 4FD and the SC codes. They are found to be the inviscid first modes and second modes whose characteristics are described by Duck et al.[21]. Note that although we compare the stability characteristics of the first and second modes with those of the boundary layer first mode and second modes, we are not using Mack's definition [2] for the first and second modes. Although higher mode instabilities with small amplitude are also found in the inviscid limit in [21], they are not found in viscous computations. While the inviscid first modes are only unstable for a small range of wave numbers when Mach number is around 3, the inviscid second modes are unstable for a large range of wave numbers and Mach numbers starting from about Mach 2.5. Accordingly, we focused on the characteristics of the inviscid second modes of the compressible Couette flow.

Figure 4 shows a unstable second mode at $M_\infty = 5.0, \alpha = 2.5$, and $Re = 10^5$ in a phase velocity eigenvalue spectrum. Although the two methods resolve the eigenvalues in the neighborhood of the triple point differently, the eigenvalues of the least stable mode resolved by both methods using 100 node points are close to convergence. Therefore, the inviscid first and second modes are considered reliable results. The disturbance eigenfunctions of the unstable mode in Fig. 4 a) and 4 b) resolved by both methods are shown in Fig. 4 c) and 4 d). The real part and the imaginary part of the second mode phase velocity at Mach 5 and Mach 10 are plotted as a function of wavenumber α in Fig. 5 a) and 5 b) for two Reynolds numbers, 5×10^5 and 10^6 respectively. Figure 5 b) shows that the dependence of the frequency of the second modes on Reynolds number is very week. Except for a small range of α, the growth rate of second modes increase with Reynolds number for a fixed Mach number, implying the inviscid nature of the unstable modes. Comparing Fig. 5 with Fig. 10 and Fig. 11 of [21], one sees that the behavior of the second modes resembles that of the second mode computed by Duck et al.[21] in the inviscid limit. Nonetheless, the mechanism of the instability is complicated by viscous effects. In the inviscid limit, Duck et al.[21] observe that the lower family modes, including second modes, change from neutrally stable to unstable as $\mathrm{Re}\{c\}$ goes from negative to positive. The results of the viscous computation in Fig. 5 show that the second modes can be stable for positive $\mathrm{Re}\{c\}$. The effects of Mach number on the second mode is more complex and will be discussed separately.

The contours of temporal amplification rates of the second modes, including the neutral stability curves, at Mach 5 and Mach 10 along with the constant frequency curves are shown in Fig. 6. The critical Reynolds numbers are approximately 90,000 and 260,000 for Mach 5 and Mach 10 respectively. Figure 6 shows that as Reynolds number increases, the range of the wave numbers corresponding to the unstable region expands while $\mathrm{Im}\{c\}$ increases. It is thus clear that the viscousity has a stabilizing effect on the second modes. This observation agrees with the results for compressible boundary layer as discussed in Mack [2].

Effects of Mach Numbers

To show the Mach number effects, we plotted the constant phase velocity curves of the second modes for a range of Mach numbers while fixing Reynolds number at 5×10^5 and 10^6, as shown in Fig. 7. In both cases, the unstable range for α expands first and then shrinks as Mach number increases. Figure 8 shows the real and imaginary part of the second modes at $Re = 5 \times 10^5$ as a function of α for various Mach numbers. Figure 8 a) shows that $\mathrm{Re}\{c\}$ of the second modes seems to reach a finite limit as Mach number increases. Figure 7 a) and 8 b) both indicate that for a fixed Reynolds number, say $Re = 5 \times 10^5$, as Mach number increases, the maximum $\mathrm{Im}\{c\}$ first increases, reaches a maximum at certain Mach number, and then decreases. The Mach number corresponding to the maximum $\mathrm{Im}\{c\}$ at $Re = 5 \times 10^5$ is about 8. For $Re = 10^6$, the Mach number is close to 10. Notice that this Mach number is around 40 in the inviscid limit as shown in Fig. 12 of [21]. We therefore see that as Reynolds number increases, the most unstable Mach number for the second mode instability also increases, but has a finite limit. For a fixed Reynolds number, the Mach number effect is in good agreement with the trend observed in other researches which emphasize on the hypersonic limit of the stability problem as mentioned in [21], that is, a general feature of hypersonic flow stability is a trend towards less unstable flows. During the search for the instabilities over a range of Mach numbers, first mode instability is also found at $Re = 10^6$. The small region

enclosed by the dashed line in Fig. 7 b) is the region where the first modes are less stable then the second modes. The first mode instability is discussed later.

Effects of Three-Dimensional Disturbances

The effects of wave angles on the second modes are illustrated in Fig. 9 and 10 at Mach 5 and Mach 10 for $Re = 10^6$. Figure 9 shows the phase velocity contours as a function of wave number α and wave angle ψ, which is $tan^{-1}(\beta/\alpha)$, at Mach 5 and Mach 10. One sees that as wave angle increases for a fixed wave number α, both Im$\{c\}$ and Re$\{c\}$ decreases. Figure 10 shows the imaginary part of the second mode as a function of wave number for different wave angles at Mach 5 and Mach 10 respectively. These figures show that three-dimensional waves are generally more stable then two-dimensional waves with an exception shown in Fig. 10 a) that there is a small range of wave number α in which three-dimensional waves with wave angles around 30° are more unstable than the two-dimensional waves. This phenomenon, however, is not seen for Mach 10. Therefore, Couette flow second modes resemble boundary layer second modes in this respect.

First mode instability

Although unstable first modes are not observed in the inviscid limit by Duck et al. [21], some first modes are shown to be neutral at certain range of wave numbers as shown in Fig. 11 a) of [21]. The range of wave numbers in which first modes are found to be less stable than the second modes as shown in Fig. 7 b) seem to coincide with the ranges where neutral first modes are found in the inviscid limit. Figure 11 shows the curve fitted maximum Im$\{c\}$ for a range of Mach numbers corresponding to both first modes and second modes at $Re = 10^6, \beta = 0$. One sees that first mode instability is much weaker than second mode instability. Furthermore it occurs in a much smaller range of Mach numbers and wave numbers. The effects of Reynolds number on the first mode instability is illustrated in Fig. 12 for $M_\infty = 2.9, \alpha = 2.5$. We see that viscous instability exists for the first modes. However, the effect of viscosity does not seem to be solely responsible for the instability since as Reynolds number further decreases, the instability disappears. This explains why the unstable first modes are not observed in Fig 7 a). The effects of wave angle for first modes at $M_\infty = 2.9, Re = 10^6$ is shown in Fig 13 for wave number α ranging from 0 to 3. When the wave number α is fixed, we see in general that both Im$\{c\}$ and Re$\{c\}$ increase as wave angle ψ increases. However, at $\alpha = 2.5$, the first modes behave like 2D modes since Im$\{c\}$ decreases with wave angle. Although the first modes for Couette flow are 3-dimensional in general, the three dimensional effects seem to be weaker than those observed for boundary layer first modes by Mack [2].

Effects of Wall Cooling

The effects of wall cooling on the first and second mode instability for Couette flow deviate from Mack's results for boundary layer. In the case of boundary layer, first modes are stabilized by wall cooling while second modes are destabilized. The effects of wall cooling on the Couette flow first modes are shown in Fig. 14 where the maximum Im$\{c\}$ (corresponding to a range of wave numbers) for $M_\infty = 2.5, Re = 10^6, \beta = 0$ is plotted against the ratio of the lower wall temperature and the adiabatic lower wall temperature. With the weak wave angle effects not accounted, the first modes are first destabilized and stabilized by wall cooling, unlike the boundary layer first modes. The effects of wall cooling on the second modes are shown in Fig. 15 for $M_\infty = 5.0, Re = 5 \times 10^5$. The second modes are first destabilized and then strongly stabilized as T_w decreases. The different response of the Couette flow first and second modes to wall cooling from their boundary layer counterparts comes from the main flow profiles. Nontheless, the instability mechanisms await further theoretical explanation.

6 Conclusion

The linear stability of compressible plane Couette flow has been investigated numerically. Two unstable modes have been found. The inviscid first modes are only unstable for a small range of Mach numbers and wave numbers. The inviscid second modes, on the other hand, is the dominant instability and unstable for a large range of Mach numbers and wave numbers. The characteristics of the inviscid second modes have been investigated in more details. The critical Reynolds numbers for Mach 5 and Mach 10 are found to be around 90,000 and 260,000, respectively. We have also shown that the inviscid second modes are in general more unstable when the disturbance is two-dimensional, while the first modes are more unstable for oblique waves. Viscous effects are stabilizing for the second modes. Viscous instability exists for the first modes. As for the Mach number effects, the trend that has been observed is that the second modes are destabilized first and then stabilized as Mach number increases. The range of Mach numbers which have the

second mode instability expands with Reynolds number but remains finite. Reducing the lower wall temperature destabilizes the first modes in general. The second modes get destabilized and then stabilized as Tw decreases. As mention previously, this work is the first step towards the understanding of stability and transition for compressible flows. We will next focus on the stability of hypersonic flow over blunt body. In attacking the problem, we will use linear stability tools developed and validated in this work as well as a DNS code by Zhong [22] and eventually a PSE code.

7 Acknowledgements

This research was supported by the Air Force Office of Scientific Research under grant numbers F49620-94-1-0019 and F49620-95-1-0405 monitored by Dr. Len Sakell.

References

[1] L. Lees and C. C. Lin. Investigation of the stability of the laminar boundary layer in a compressible fluid. *NACA Tech. Note 1115*, 1993.

[2] L. M. Mack. Boundary-layer linear stability theory. *AGARD Rep. 704,3-1*, 1984.

[3] A. R. Wazzan, T. T. Okamura, and A. M. O. Smith. Spatial and temporal stability charts for the falkner-skan boundary layer profiles. *McDonnell-Douglas Aircraft Co., Rept. No. DAC-67086*, 1968.

[4] M. R. Malik and S. A. Orzag. Efficient computation of the stability of three-dimensional compressible boundary layers. *AIAA Rep. No. 81-1277*, 1981.

[5] H. Bippes and B. Müller. Disturbance growth in an unstable three-dimensional boundary layer. *In Numerical and Physical Aspects of Aerodynamic Flows IV. Ed.*, pages 345–58, 1990.

[6] W. S. Saric. Physical description of boundary-layer transition: Experimental evidence. *AGARD Rep. No. 793*, 1994.

[7] H. L. Reed and W. S. Saric. Linear disturbances in hypersonic, chemically reacting shock layers. *AIAA Journal*, 32(7):1384–1393, 1989.

[8] A. M. O. Smith and N. Gamberoni. Transition, pressure gradient, and stability theory. *Rep. No. ES. 26388, Douglas Aircr. Co., Inc*, 1956.

[9] J. L. Van Ingen. A suggested semi-emporical method for the calculation of the boundary layer transtion region. *Rep. Nos. VTH. 71 and 74, Dept. Aeronaut. Eng., Univ. Technol. Delft, Netherlands*, 1956.

[10] L. Kleiser and T. A. Zang. Numerical simulation of transition in wall-bounded shear flows. *Annu. Rev. Fluid Mech.*, 23:495–537, 1991.

[11] F. P. Bertolotti. Compressible boundary layer stability analyzed with the pse equations. *AIAA-91-1637-CP*, 1991.

[12] F. P. Bertolotti, Th. Herbert, and P. R. Spalart. Linear and nonlinear stability of the blasius boundary layer. *J. Fluid Mech.,vol 242;441-74*, 1992.

[13] Th. Herbert. Parabolized stability equations. *AGARD Rep. No.793*, 1994.

[14] M. R. Malik. Numerical methods for hypersonic boundary layer stability. *Journal of Computational Physics*, 86:376–413, 1990.

[15] V. A. Romanov. Stability of plane-parallel couette flow. *Functional Anal. Applics. 7, 137*, 1973.

[16] G. I. Taylor. Fluid friction between rotating cylinder. *Proc. R. SOc. Lond., A 157, 546*, 1989.

[17] J. M. Robertson. On turbulent plane-couette flow. *In Proc. 6th Mid. Western Conf. on Fluid Mech., University of Texas,p. 169*, 1959.

[18] W. Glatzel. Sonic instability in supersonic shear flows. *Mon. Not. R. Astron. Soc., 233, 795*, 1988.

[19] W. Glatzel. The linear stability of viscous compressible plane couette flow. *J. Fluid Mech. 202, 515*, 1989.

[20] J. J. Girard. Study of the stability of compressible couette flow. *PhD dissertation, Washington State University*, 1988.

[21] P. M. Duck, G. Erlebacher, and M. Y. Hussaini. On the linear stability of compressible plane couette flow. *J. Fluid Mech., vol. 258. pp 131-165*, 1994.

[22] X. Zhong. Direct numerical simulation of hypersonic boundary layer transition over blunt leading edges, part i: A new numerical method and validation. *AIAA-97-0755*, 1997.

[23] S. C. Reddy, P. J. Schmid, and D. S. Henningson. Pseudospectra of the orr-sommerfeld operator. *SIAM J. Appl. Maths 53, 15*, 1993.

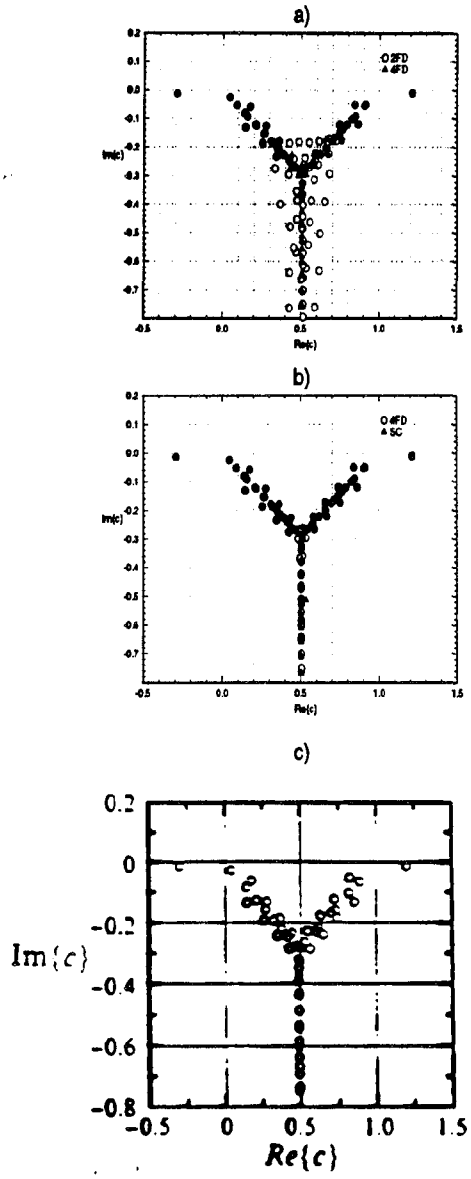

Figure 1: Phase velocity spectrum at $M_\infty = 2.0, Re = 2 \times 10^5, \alpha = 0.1$ and N=100: a) comparison between 2FD and 4FD, b) comparison between 4FD and SC, c) Duck et al's result at the same conditions.

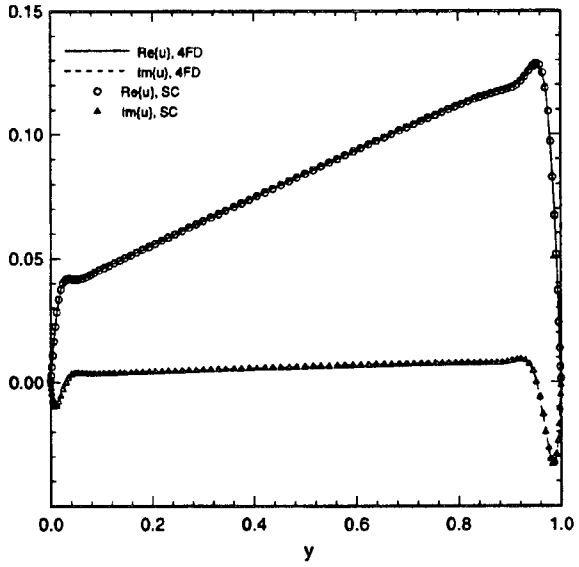

Figure 2: Eigenfunction ($\widehat{u}$) of the least stable mode (the first mode) resolved by the 4FD and SC methods at $M_\infty = 2.0, Re = 2 \times 10^5, \alpha = 0.1$ and N=100.

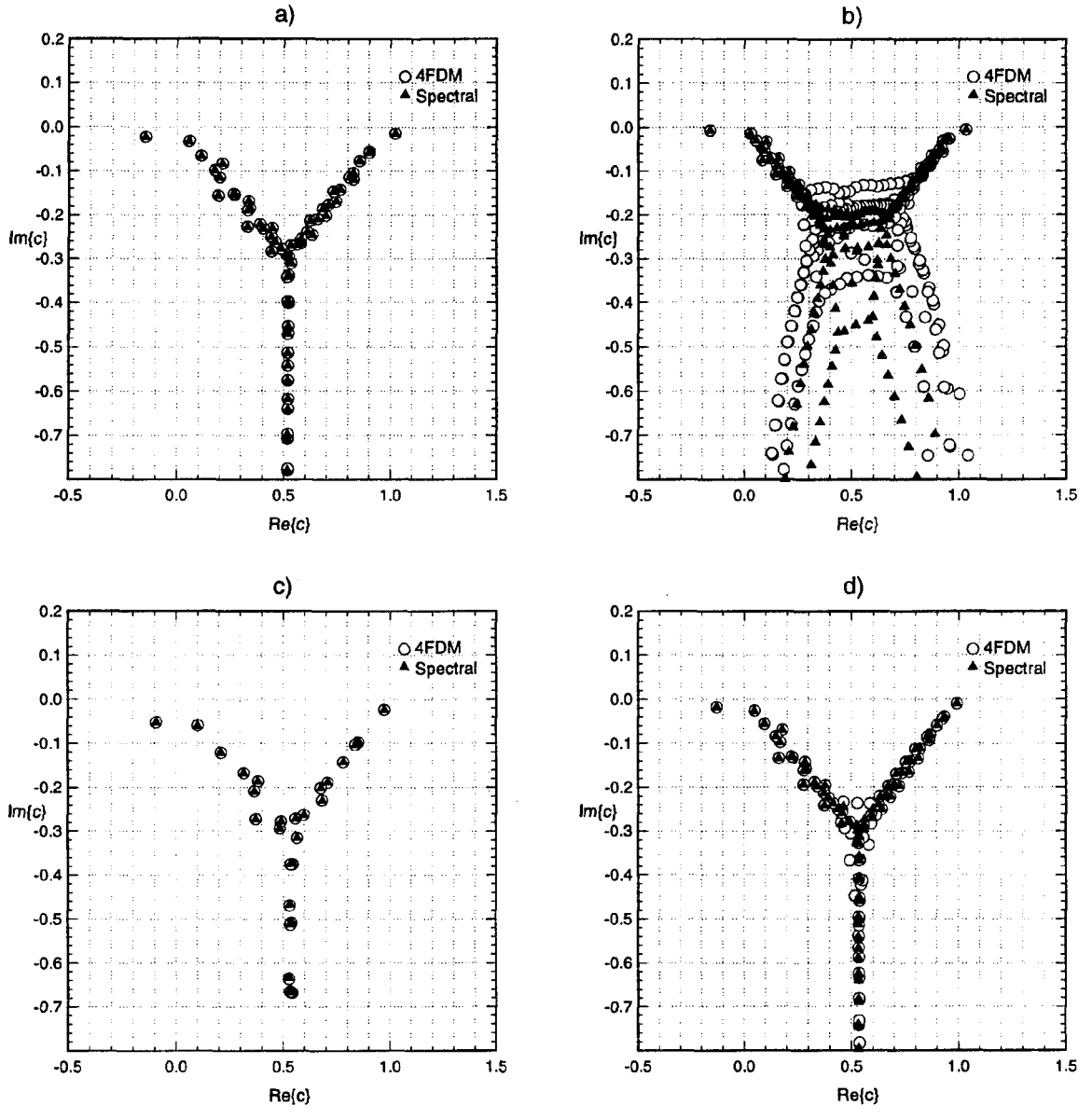

Figure 3: Phase velocity spectra at $\alpha = 0.1$: a) $M_\infty = 5.0$, and $Re = 5 \times 10^5$, b) $M_\infty = 5.0$, and $Re = 5 \times 10^6$, c) $M_\infty = 10.0$, and $Re = 5 \times 10^5$, d) $M_\infty = 10.0$, and $Re = 5 \times 10^6$.

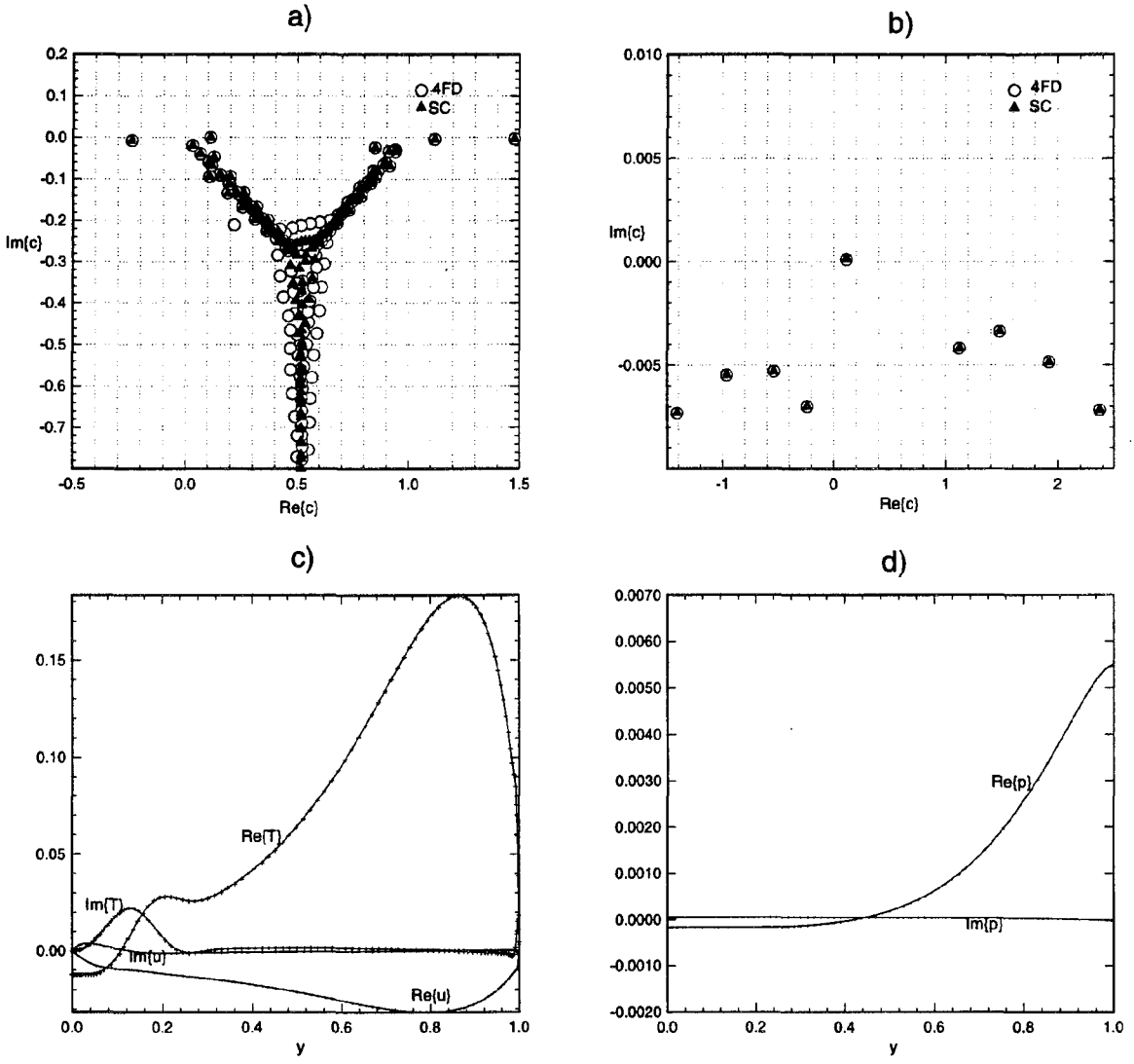

Figure 4: The unstable second mode at $M_\infty = 5.0$, $\alpha = 2.5$ and $Re = 10^5$: a) phase velocity Im{c} spectrum resolved by the 4FD and the spectral collocation method, using 150 grid point, b) a blowup of the spectrum, c) and d) disturbance eigenfunctions of the unstable mode computed by both methods: the 4FDM '—', the spectral collocation method '+', using 100 grid points.

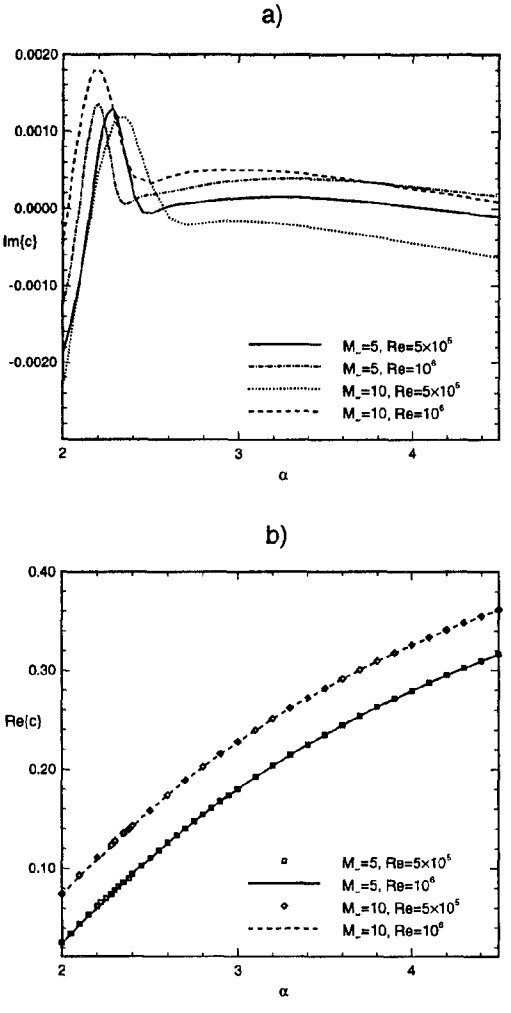

Figure 5: The eigenvalues of the second modes as a function of α: a) Im$\{c\}$, b) Re$\{c\}$.

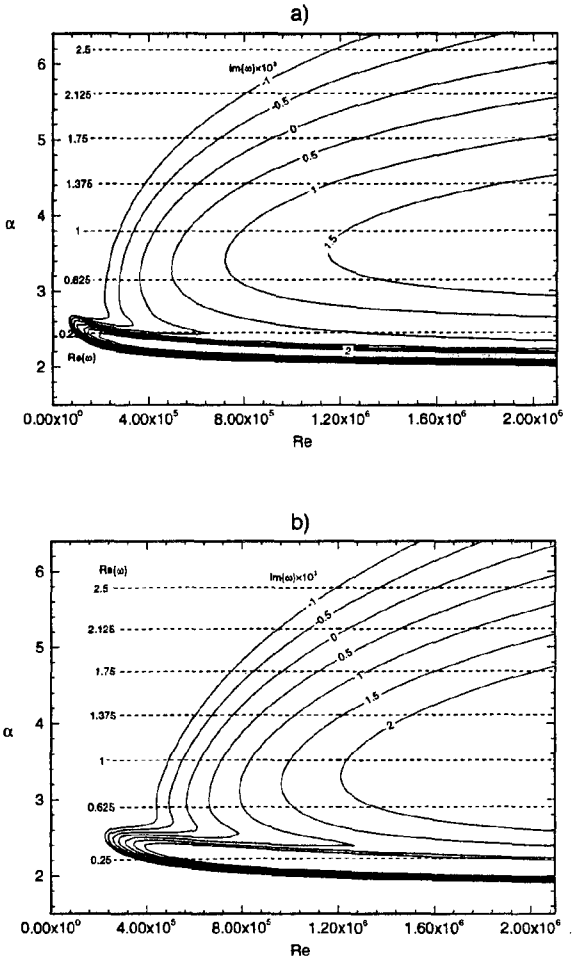

Figure 6: The second mode growth rate contours as a function of α and Reynolds number: a) $M_\infty = 5.0$, b) $M_\infty = 10.0$.

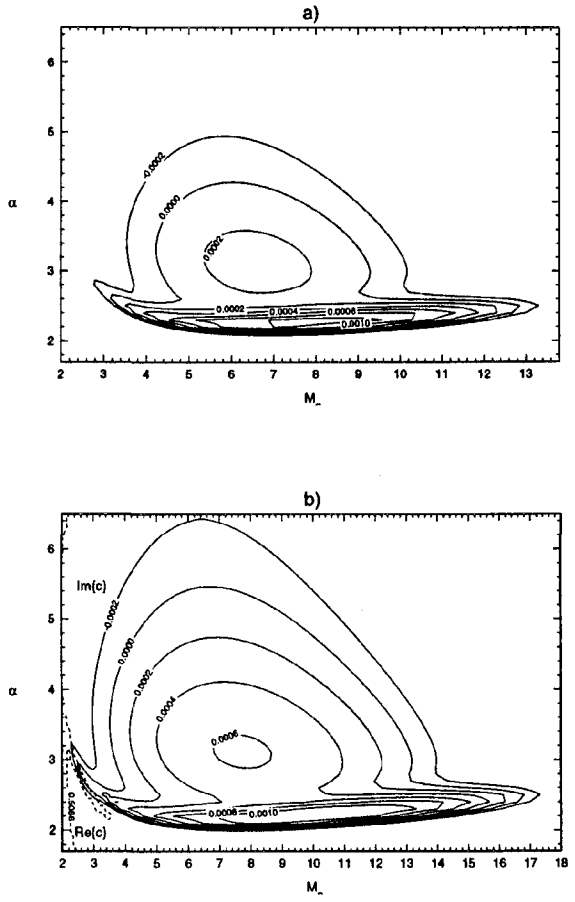

Figure 7: The second mode $\mathrm{Im}\{c\}$ contours as a function of α and Mach number: a) $Re = 5 \times 10^5$, b) $Re = 10^6$.

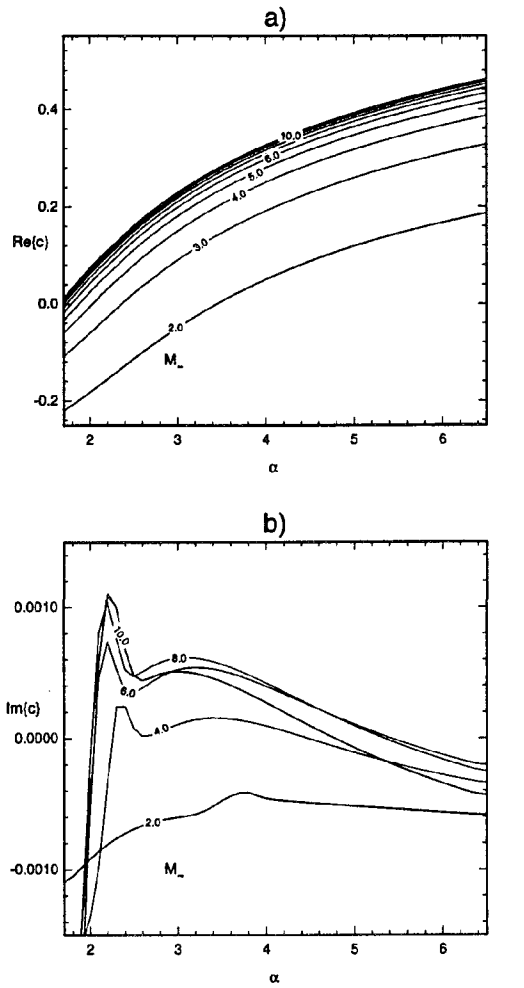

Figure 8: The second modes as a function of α and Mach number, for the case of $Re = 5 \times 10^5$: a) $\mathrm{Re}\{c\}$ for various Mach numbers, b) $\mathrm{Im}\{c\}$ for various Mach numbers.

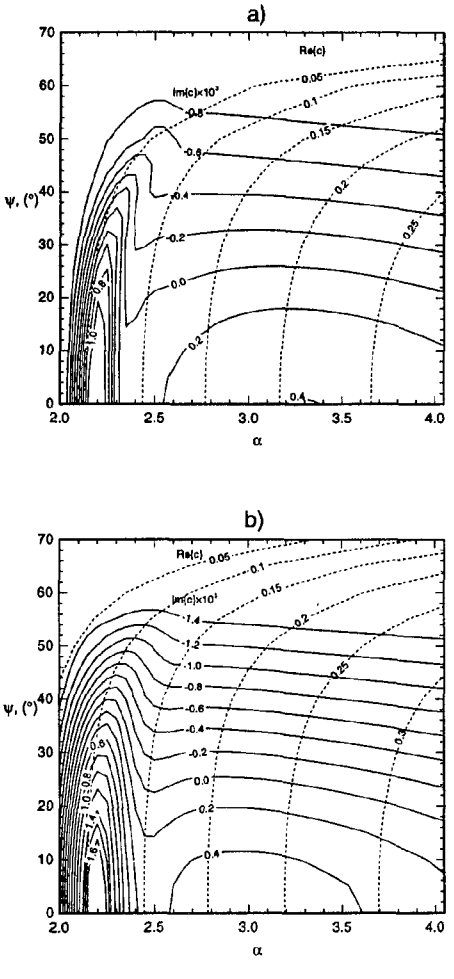

Figure 9: Contours of $\mathrm{Im}\{c\}\times 10^3$ and $\mathrm{Re}\{c\}$ of the second modes at $Re = 10^6$ as a function of wave angle ψ and α: a)$M_\infty = 5.0$, b) $M_\infty = 10.0$.

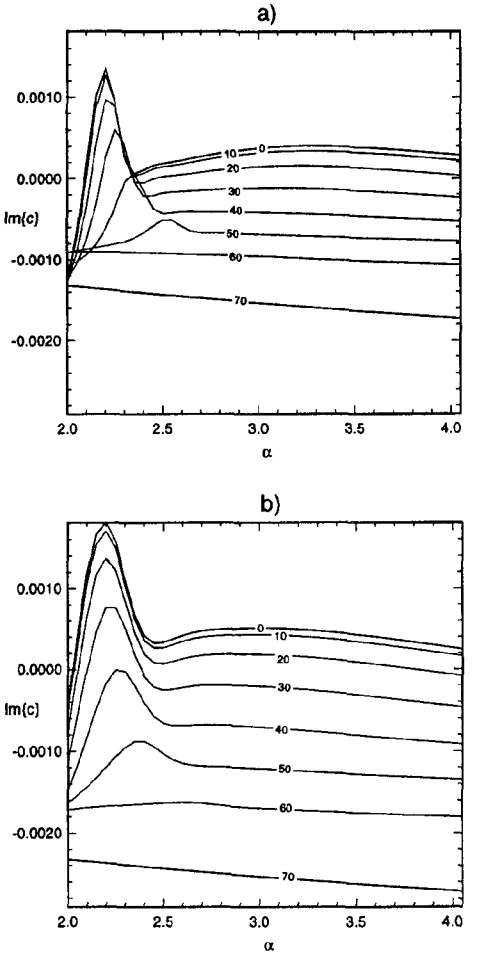

Figure 10: $\mathrm{Im}\{c\}$ of the second modes for different wave angles at $Re = 10^6$: a) $M_\infty = 5.0$, b) $M_\infty = 10.0$.

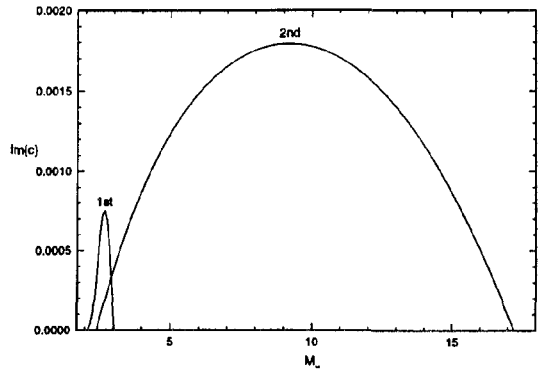

Figure 11: Maximum $\mathrm{Im}\{c\}$ of the first modes and the second modes for different Mach numbers at $Re = 10^6$ (curve fit results).

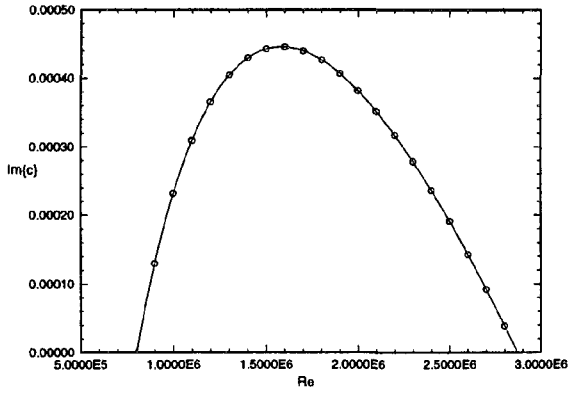

Figure 12: The effects of Reynolds number on the first mode instability. $M_\infty = 2.9, \alpha = 2.5$.

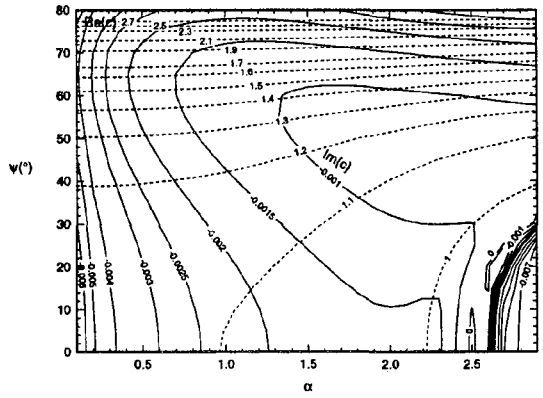

Figure 13: The effects of wave angle on the first modes. $M_\infty = 2.9, Re = 10^6$.

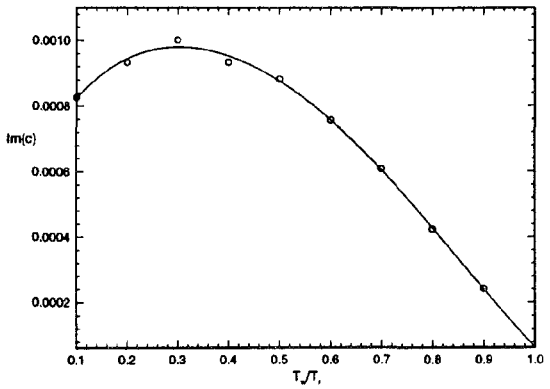

Figure 14: The effects of wall-cooling on the first mode instability. $M_\infty = 2.5, Re = 10^6, \beta = 0.0$.

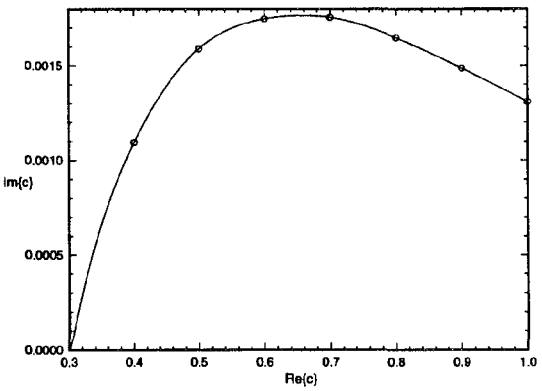

Figure 15: The effects of wall-cooling on the second mode instability. $M_\infty = 5.0, Re = 5 \times 10^5$.